

Article

Ionic Conductivity Analysis of NASICON Solid Electrolyte Coated with Polyvinyl-Based Polymers

Tiago Afonso Salgueiro ^{1,2}, Rita Carvalho Veloso ², João Ventura ², Federico Danzi ¹ and Joana Oliveira ^{1,2,*}

¹ Associate Laboratory for Energy, Transports and Aerospace (LAETA/INEGI), Faculty of Engineering, University of Porto, 4200-465 Porto, Portugal; up201704006@up.pt (T.A.S.); fdanzi@fe.up.pt (F.D.)

² Institute of Physics and Advanced Materials, Nanotechnology and Photonics (IFIMUP), Faculty of Sciences, University of Porto, 4169-007 Porto, Portugal; ana.rita.veloso@fc.up.pt (R.C.V.); joventur@fc.up.pt (J.V.)

* Correspondence: jespain@fe.up.pt

Abstract: The global environmental crisis necessitates reliable, sustainable, and safe energy storage solutions. The current systems are nearing their capacity limits due to the reliance on conventional liquid electrolytes, which are fraught with stability and safety concerns, prompting the exploration of solid-state electrolytes, which enable the integration of metal electrodes. Solid-state sodium-ion batteries emerge as an appealing option by leveraging the abundance, low cost, and sustainability of sodium. However, low ionic conductivity and high interfacial resistance currently prevent their widespread adoption. This study explores polyvinyl-based polymers as wetting agents for the NASICON-type NZSP ($\text{Na}_3\text{Zr}_2\text{Si}_2\text{PO}_{12}$) solid electrolyte, resulting in a combined system with enhanced ionic conductivity suitable for Na-ion solid-state full cells. Electrochemical impedance spectroscopy (EIS) performed on symmetric cells employing NZSP paired with different wetting agent compositions demonstrates a significant reduction in interfacial resistance with the use of poly(vinyl acetate)—(PVAc)- based polymers, achieving an impressive ionic conductivity of 1.31 mS cm^{-1} at room temperature, 63.8% higher than the pristine material, notably reaching 7.36 mS cm^{-1} at 90°C . These results offer valuable insights into the potential of PVAc-based polymers for advancing high-performance solid-state sodium-ion batteries by reducing their total internal resistance.

Keywords: solid-state sodium-ion batteries; NASICON; NZSP; symmetric cells; ionic conductivity; electrochemical impedance spectroscopy; polyvinyl-based polymers; wetting agents



Citation: Salgueiro, T.A.; Veloso, R.C.; Ventura, J.; Danzi, F.; Oliveira, J. Ionic Conductivity Analysis of NASICON Solid Electrolyte Coated with Polyvinyl-Based Polymers. *Batteries* **2024**, *10*, 157. <https://doi.org/10.3390/batteries10050157>

Academic Editors: Junnan Hao and Seiji Kumagai

Received: 20 February 2024

Revised: 8 April 2024

Accepted: 24 April 2024

Published: 3 May 2024



Copyright: © 2024 by the authors. Licensee MDPI, Basel, Switzerland. This article is an open access article distributed under the terms and conditions of the Creative Commons Attribution (CC BY) license (<https://creativecommons.org/licenses/by/4.0/>).

1. Introduction

The urgent need to meet the ever-increasing global energy demands with efficient and sustainable energy storage solutions has driven the quest for alternatives to present lithium-ion batteries. While these batteries have been instrumental in various applications, they face challenges such as limited energy density, finite cycle life, and environmental concerns related to lithium extraction and processing [1,2]. In response, solid-state batteries, particularly sodium-ion systems, have emerged as promising alternatives. Solid-state batteries employ solid electrolytes that allow for the use of metallic anodes, resulting in higher energy densities and prolonged cycle lives [3]. Beyond performance, these devices offer other advantages such as eliminating the risk of electrolyte leakage, allowing for the creation of simpler designs that can more easily be adapted to each individual application [4]. Solid-state electrolytes are also more chemically and mechanically stable, offering greater resistance to dendrite formation and penetration [5].

Solid-state sodium-ion batteries (SSIBs) combine the advantages of solid-state technology with the abundant and widely distributed nature of sodium, making them more sustainable and cost-effective compared to their lithium-ion counterparts [2]. However, SSIBs encounter performance-related challenges that need to be overcome in order to make them a true alternative to lithium-based systems. The lack of performance arises mainly from the larger sodium ionic radius, which hinders ionic mobility and adsorption and

causes larger volumetric variations during the charge/discharge process, ultimately leading to lower capacity and cycling stability [4,6]. Another major hurdle is the poor quality of the electrode/electrolyte interface. Since both the electrode and the electrolyte are solid materials, the effective contact area is greatly reduced when compared to liquid electrolyte systems, resulting in a reduction in the overall ionic conductivity of the cell.

The sodium-ion solid-state electrolyte $\text{Na}_3\text{Zr}_2\text{Si}_2\text{PO}_{12}$ (NZSP) is a NASICON (Na super ionic conductor-) type material, widely recognized as one of the most promising in SSIB research due to its 3D paths for the movement of sodium ions and strong covalent framework [7]. NZSP has an initial reported high ionic conductivity of 0.67 mS cm^{-1} at room temperature, which has since been increased to as high as $\approx 2 \text{ mS cm}^{-1}$ through novel manufacturing techniques, such as solution-assisted solid-state reaction, spark plasma sintering, sol-gel reduction, and an additive-assisted solid-state process, although the traditional solid-state method remains the simpler procedure [8–12]. The stable NASICON structure offers mechanical strength and some resistance to dendrite formation [5,13]. The chemical and thermodynamic stability and resistance to air and humidity of NZSP also have the added benefit of making it compatible with a wide range of electrode materials [14,15]. The main challenge currently hindering the application of NZSP as a solid electrolyte in SSIBs is the high interfacial resistance at the electrode/electrolyte interface, resulting in a decrease in ionic mobility and total ionic conductivity of the cell [5]. Considerable efforts have been made to overcome this challenge, namely, by doping elements in bulk and adjusting the chemical composition of the grain boundary [7,11]. Leng et al. successfully decreased the grain-boundary resistance and achieved a high ionic conductivity of 1.36 mS cm^{-1} for a Mg^{2+} -doped NZSP [16]. Introducing additional interphases, such as ionic liquids, liquid electrolytes, or polymers as wetting agents, is another established efficient strategy used to modify the interface of NZSP and achieve more intimate electrode contact and stability [14,17]. Fu et al. employed a coating of epoxy resin to F^- -assisted NZSPF_x and obtained an ionic conductivity of 0.67 mS cm^{-1} at ambient temperature, paired with an improvement in dendrite growth inhibition [18].

In this work, three wetting agents: Poly(vinyl alcohol) (PVA), poly(vinyl acetate) (PVAc), and commercial PVAc-based wood glue are analyzed in symmetric cells with gold blocking electrodes, with the aim of finding the configuration that results in the lowest total resistance when applied to the NZSP solid electrolyte.

Ion conduction in polymer electrolytes is generally understood to occur mainly in the amorphous region of the host polymer matrix, where the molecular chains move more freely than in the crystallized region and oscillate above the glass transition temperature, enabling ion conduction [19]. Polymer electrolytes have good flexibility for compensating electrode volume changes during battery operation and low interfacial resistance, although they typically suffer from low ionic conductivity at ambient temperature and less stability, compared to ceramic electrolytes [5].

Polyvinyl-based polymers have been shown in various studies to have good performance as dielectrics in supercapacitors [20] and as a host polymer in solid polymer electrolytes [21]. Bhargav et al. synthesized an NaBr:PVA polymer electrolyte with an ionic conductivity of $1.36 \times 10^{-4} \text{ S cm}^{-1}$, while Sasikumar et al. successfully implemented PVAc in a P(VdF-HFP)-LiTFSI-EC complex, resulting in a blend solid polymer electrolyte with a higher ionic conductivity of 1.1 mS cm^{-1} [22,23]. These limited but promising results regarding polyvinyl-based electrolytes provide the impetus for the investigation of these polymers in the role of wetting agents for solid-state electrolytes, such as NZSP, integrating the advantages of ceramic and polymer. The use of glycerin as a plasticizer for these polymers is also considered, due to its successful implementation in sodium-ion polymer electrolytes, as a means to provide increased mobility for sodium ions by reducing the crystallinity of the polymer electrolytes and increasing the prevalence of the amorphous region [5,20,24].

2. Materials and Methods

2.1. Material Preparation

The NZSP ceramic electrolyte was used as-purchased from 4 to One Co., Ltd., Ulju-gun Ulsan, Republic of Korea. This pellet is fabricated in mass-production facilities via the solid-state reaction route, which includes consecutive processing steps of $\text{Na}_3\text{PO}_4 \cdot 12\text{H}_2\text{O}$, SiO_2 and ZrO_2 precursor mixing, calcination at 400 °C and 1000 °C, compaction, and sintering at 1230 °C, resulting in a circular-shaped pellet with 20 mm diameter and 1 mm thickness with a bulk density of 3.03 g cm^{-3} (92% of the theoretical value) and a high ionic conductivity of $\approx 0.8 \text{ mS cm}^{-1}$ [10,25,26].

The SUPERTITE® (Ideias adhesivas Unecol S.L., Valencia, Spain) PVAc-based wood glue and commercial 95% glycerol-content glycerin were used as-obtained from general stores. Poly(vinyl alcohol) ($[-\text{CH}_2\text{CHOH}-]_n$; $M_W = 89,000\text{--}98,000$, 99+% hydrolyzed) was acquired from Sigma-aldrich (CAS No.: 9002-89-5) and dispersed in ultrapure water (12% wt.) at 85 °C for 3 h until complete dissolution. Poly(vinyl acetate) ($[\text{CH}_2\text{CH}(\text{O}_2\text{CCH}_3)]_n$; M_W ca. 170,000) was acquired from Sigma-aldrich (CAS No.: 9003-20-7) and dispersed in Dimethylformamide (15% wt.) over 4 h at 50 °C until complete dissolution.

Each composition of an NZSP pellet coated with a polymeric wetting agent underwent testing in a symmetric cell configuration with gold ion-blocking electrodes, aiming to assess the corresponding impedance response. Beyond blocking ion transfer at the electrode/electrolyte interface, gold was employed in this role because of its high electrical conductivity and stability [27]. An average wetting agent mass loading of 45 mg cm^{-2} was coated on each side of the NZSP pellet using the doctor blade technique. The different wetting agent + pellet combinations were placed between the gold electrodes and sealed with Teflon tape.

2.2. Experimental Methods

All galvanostatic measurements were conducted with a Gamry interface 1010E potentiostat (Gamry Instruments, Warminster, PA, USA), using a two-electrode configuration. Electrochemical impedance spectroscopy (EIS) was performed in the 0.1 Hz to 10^6 MHz range, from which the ionic conductivity and total resistance values were obtained for each cell configuration by fitting the obtained Nyquist plots to the corresponding equivalent circuit. For temperature variation tests where close control and monitoring of temperature and humidity were required, a TMAX-80L environmental battery test chamber from Xiamen Tmax Battery equipments Ltd. (Xiamen City, Fujian Province, China) was employed.

Chemical characterization of the polymeric PVA-based wetting agents was performed via Fourier transform infrared with attenuated total reflection (FTIR-ATR) spectroscopy, using a Perkin Elmer spectrum BX system spectrometer in transmission mode, at the $4000\text{--}400 \text{ cm}^{-1}$ wavenumber range. SEM morphological measurements of the NZSP electrolyte surface were performed using a Phillips FEI/Quanta 400 FEG high resolution scanning electron microscope. From the characteristic X-rays generated during the SEM imaging acquisition, an EDS diffractogram was also produced under a working voltage of 15 keV in order to confirm that the NZSP solid electrolyte has the expected composition.

3. Results and Discussion

3.1. FTIR Chemical Characterization

FTIR-ATR spectra of the different polymeric matrices are recorded at room temperature and displayed in Figure 1. For pure PVAc and PVAc-based glue, identical peaks can be observed for both polymer matrices, especially in the $1500\text{--}450 \text{ cm}^{-1}$ magnified range. The peaks located at 1434 cm^{-1} and 1372 cm^{-1} are attributed to CH_2 and CH_3 bending vibrations, respectively [28]. A typical band of PVAc located at 1230 cm^{-1} , from the C-O stretching, is identified in both polymers [29]. The peaks at 1105 cm^{-1} and 1029 cm^{-1} were associated with C-C-C, C-C-O and C-C symmetric stretching vibration, typically, as well as for PVAc polymers [28–30]. The smaller bands at 947 cm^{-1} and 801 cm^{-1} are more pronounced in the pristine polymer due to the CH_3 and CH_2 rocking vibrations.

The band between 686–568 cm^{-1} is related to the acetate group, from the structural skeleton of PVAc, assigned as bending vibration of the CH_3COO group [28]. In fact, the resulting spectra exhibit similar band profiles without a band shift, confirming the PVAc base in the composition of the commercial glue, and are in good agreement with the found literature.

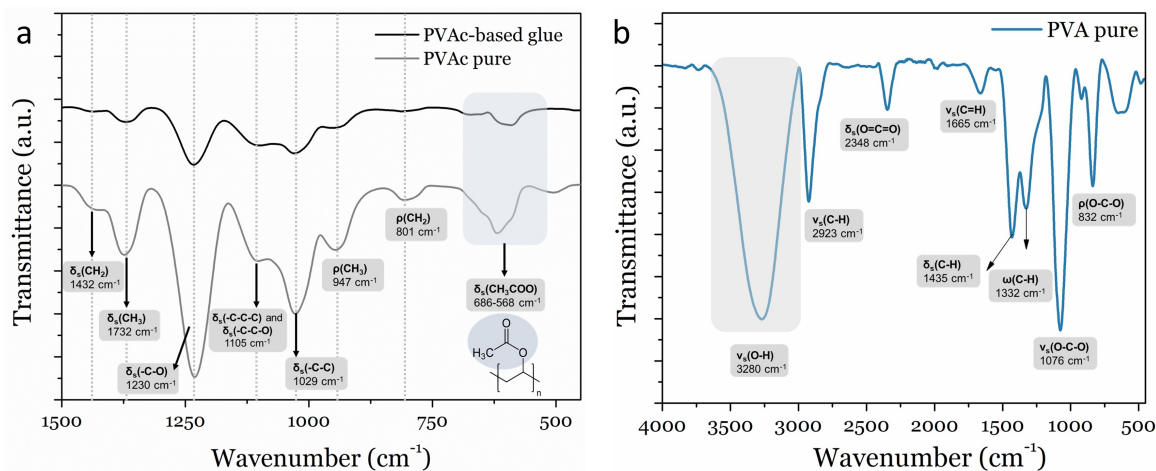


Figure 1. FTIR-ATR absorption spectra of (a) PVAc and PVAc-based glue in the magnified range of 1500–450 cm^{-1} and (b) PVA in the 4000–450 cm^{-1} range. The symbols ν , δ , ω , and ρ represent stretching, bending, wagging, and rocking vibrations, respectively.

In Figure 1b, a common peak profile for the PVA spectrum was obtained in the 4000–400 cm^{-1} range at room temperature. A broad band located at 3280 cm^{-1} corresponds to the O-H stretching vibration (3550–3200 cm^{-1}) due to the water molecules and/or PVA intramolecular hydrogen bonds [31]. The peaks at 2923 cm^{-1} , 1435 cm^{-1} , and 1332 cm^{-1} were ascribed to the stretching, bending, and wagging C-H vibrations [32], respectively, while those located at 2348 cm^{-1} are associated with O=C=O bending vibration due to CO_2 adsorption. The peaks detected at 1660 cm^{-1} and at 1076 cm^{-1} correspond to C=O stretching vibrations from the acetate group and C-O stretching vibrations, all associated with the PVA structure [32–34]. The intense peak at 832 cm^{-1} is attributed to the PVA structural skeleton, assigned as C-H rocking vibrations [32].

3.2. EIS Results at Room Temperature

3.2.1. Pristine NZSP

The performance of the different wetting agent solutions can only be evaluated after establishing the pristine NZSP baseline without any wetting agent. First, an EDS diffractogram of the NZSP pellet was obtained to confirm that it has the expected composition and relative element percentage, as displayed in Figure 2b.

The electrochemical performance baseline was obtained by conducting an EIS test on an Au/NZSP/Au symmetric cell and the subsequent analysis of the resulting Nyquist plot presented in Figure 2a. This plot was then fitted to the corresponding equivalent circuit for this cell configuration, which encompasses a resistor R_1 that accounts for the ohmic resistance of all the components of the cell, followed by a parallel of another resistor, R_2 , and a constant phase element, CPE_1 , that represent the grain-boundary resistance, both in the bulk and at the electrode/electrolyte interface, associated with charge accumulation through the double layer capacitance (EDLC) [35,36]. By adding the values obtained for R_1 and R_2 , the total resistance of the cell, $R_t = 67.7 \text{ k}\Omega$, was calculated. This value can then be used to calculate the ionic conductivity of the system, by using Equation (1), where t represents the thickness, and A represents the surface area of the solid electrolyte pellet:

$$\sigma = \frac{t}{R_t A} \quad (\text{S/cm}) \quad (1)$$

The markedly high value obtained for the total resistance corresponds, in turn, to an ionic conductivity of $6.03 \times 10^{-4} \text{ mS cm}^{-1}$, which is much lower than both the initially reported conductivity of 0.67 mS cm^{-1} and the value indicated by the manufacturer for this specific NZSP pellet of $\approx 0.8 \text{ mS cm}^{-1}$ [8,10]. This discrepancy is due to the fact that this conductivity in ideal conditions is obtained by coating the ion-blocking electrodes onto the NZSP pellet directly, using techniques such as sputtering, thus minimizing the electrode/electrolyte interfacial resistance [36,37]. In this study, the focus is on reducing the interfacial resistance of NZSP under practical real-world cell operating conditions, where the effective electrode/electrolyte contact surface area is smaller compared to the electrode deposition case. The numerous microscopic irregularities expected to be present on the surface of the solid NZSP pellet are evidenced by the high magnification SEM images shown in Figure 2 and are responsible for the imperfect contact with the electrodes and the high interfacial resistance measured [10]. Incorporating polymeric wetting agents can effectively mitigate the effect of these defects and microscopic irregularities by wetting/adhering to the electrode surface and creating a more homogenous interface, improving the electrode/electrolyte interface properties and causing a reduction in interfacial resistance, thereby increasing the overall ionic conductivity, as is evidenced in the following sections [38].

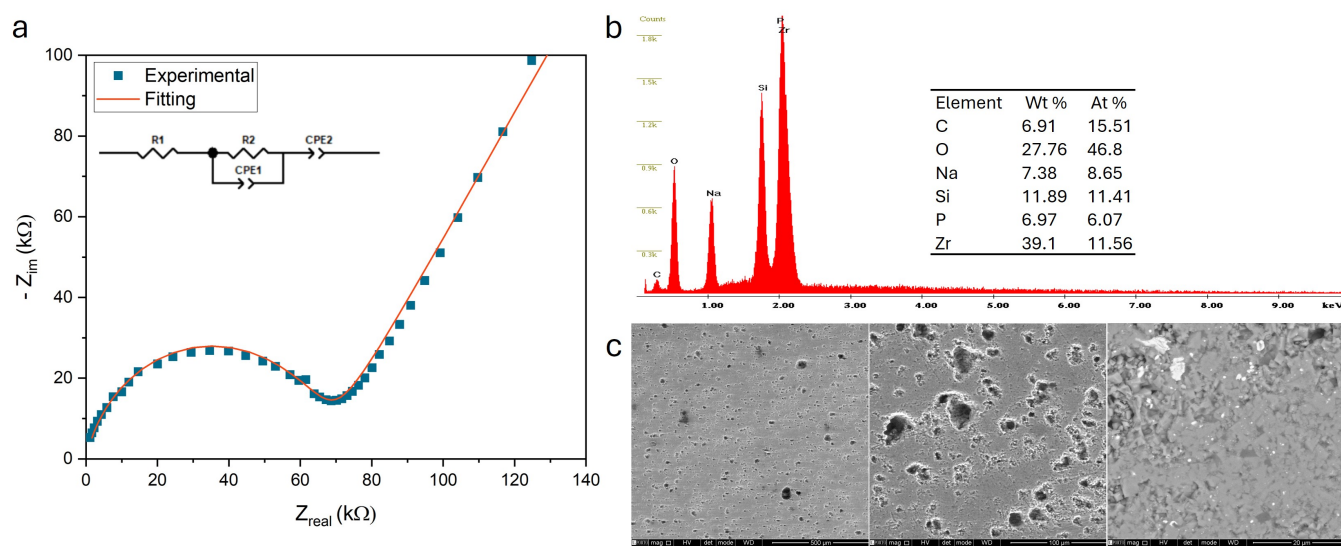


Figure 2. (a) Nyquist diagram for Au/NZSP/Au symmetric cell fitted to the respective equivalent circuit (inset). (b) EDS diffractogram of the NZSP pellet with relative weight (wt.%) and atomic (at.%) percentage table inset. (c) SEM imaging of the NZSP pellet surface with $200\times$ magnification ($500 \mu\text{m}$ scale), $1000\times$ magnification ($100 \mu\text{m}$ scale) and $5000\times$ magnification ($20 \mu\text{m}$ scale).

3.2.2. Wetting Agent Performance at Room Temperature

Three polymeric materials were considered as potential wetting agents: PVA, PVAc-based glue, and PVAc. The different NZSP+polymer combinations were tested via EIS spectroscopy of the Au/NZSP+wetting agent/Au symmetric cells, obtained at room temperature. After fitting the data to the corresponding equivalent circuit model, the best wetting agent candidate is the one that results in the lowest total resistance and highest ionic conductivity. The Nyquist plots and fittings for each wetting agent+NZSP composition, at ambient temperature, are presented in Figure 3. From these plots and the fitting parameters, the total resistance and ionic conductivity values were calculated, as shown in Table 1.

All the tested polyvinyl-based polymers were able to effectively improve the interfacial contact between the NZSP and the gold electrodes and demonstrated improved ionic conductivity without any observed chemical instability. Of the three, PVAc-based glue stood out as having the best performance, closely followed by PVA and PVAc at a distant third.

Coating PVAc-based glue onto the NZSP solid electrolyte resulted in an impressive ionic conductivity of 1.31 mS cm^{-1} , more than 2000 times larger than the one obtained with the pristine pellet and, remarkably, 63.8% higher than the maximum ionic conductivity for the NZSP pellet, indicated by the manufacturer [10]. Using PVAc-based glue as a wetting agent for NZSP is a simple and cost-effective way of not only unlocking the full ionic conductivity potential of the solid electrolyte, dramatically reducing the interfacial resistance at the electrode/electrolyte interface, but also attaining a higher ionic conductivity than the pristine material.

In an effort to further improve the performance of PVAc-based glue, glycerin was employed as a plasticizer and mixed with PVAc-based glue in different percentages, with the results presented in Figure A2 showing a clear tendency for ionic conductivity improvement, with the decrease in glycerin content, culminating in a maximum value of 1.16 mS cm^{-1} , obtained with 10% glycerin content. This value is very close but crucially below the one attained with a cell employing only PVAc-based glue (1.31 mS cm^{-1}), leading to the conclusion that, contrary to expectations, adding glycerin to PVAc-based glue does not result in an improvement in ionic conductivity.

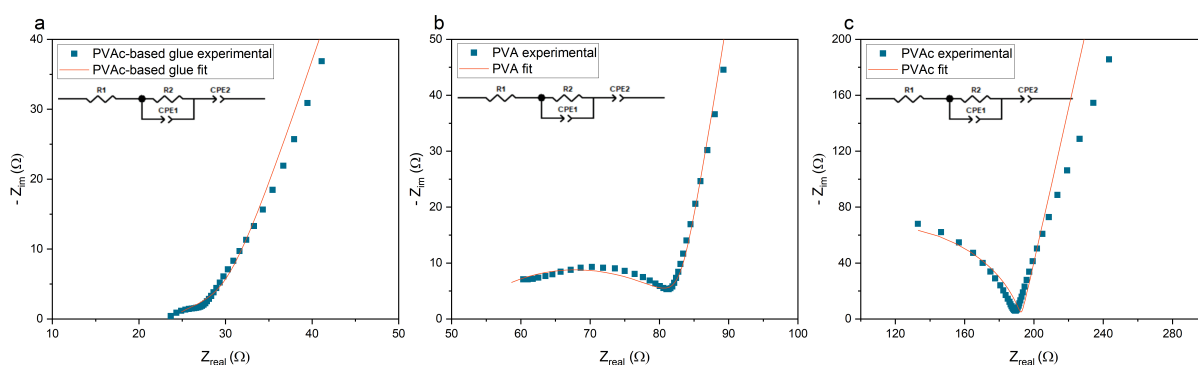


Figure 3. Nyquist diagram with equivalent circuit fitting (inset) for (a) PVAc-based glue, (b) PVA, (c) PVAc symmetric Au/NZSP + wetting agent/Au cells.

Table 1. Total resistance and ionic conductivity for the pristine NZSP pellet, compared to the pellet coated with the three wetting agents, in order of increasing ionic conductivity.

Wetting Agent	Total Resistance (Ω)	Ionic Conductivity (mS cm^{-1})
Pristine NZSP	6.77×10^4	6.03×10^{-4}
Pure PVAc	192.65	0.21
Pure PVA	83.39	0.31
PVAc-based glue	31.23	1.31

3.3. Temperature Variation

A subsequent test was performed to ascertain whether these polymers can maintain satisfactory performance and chemical stability at the elevated temperatures commonly encountered in real world battery operation. Three symmetric cells employing PVA, PVAc, and PVAc-based glue were tested inside an environmental battery test chamber in the $25 \text{ }^\circ\text{C}$ to $90 \text{ }^\circ\text{C}$ temperature range. The results are displayed in Figure 4, both in terms of direct EIS results and in the form of ionic conductivity as a function of temperature.

The obtained results are in accordance with the ones obtained at ambient temperature, with the cell employing PVAc-based glue still displaying the lowest total resistance and highest ionic conductivity at every step of the tested temperature range, outperforming both pristine PVA and PVAc. This large gulf in performance between the glue and the pristine polymers, mainly PVAc, can likely be attributed to the different composition of the glue, highlighted in Section 3.1.

PVAc-based glue reached an admirable maximum ionic conductivity of 7.36 mS cm^{-1} at $90 \text{ }^\circ\text{C}$, 5.6 times larger than that obtained at $25 \text{ }^\circ\text{C}$. Although high temperatures typically

increase the prevalence of the amorphous region of the polymer matrix, increasing ionic conductivity, this temperature is higher than the glass transition temperature of PVA, typically in the 75–85 °C range, a transition that predominantly affects the amorphous region of the polymer [21,22,39]. Additionally, high temperatures promote solvent evaporation, causing the polymer to become hardened and brittle [40]. However, as shown in Figure A1, upon returning to ambient temperature, the cell still displayed similar performance in terms of resistance and ionic conductivity, as it did before testing.

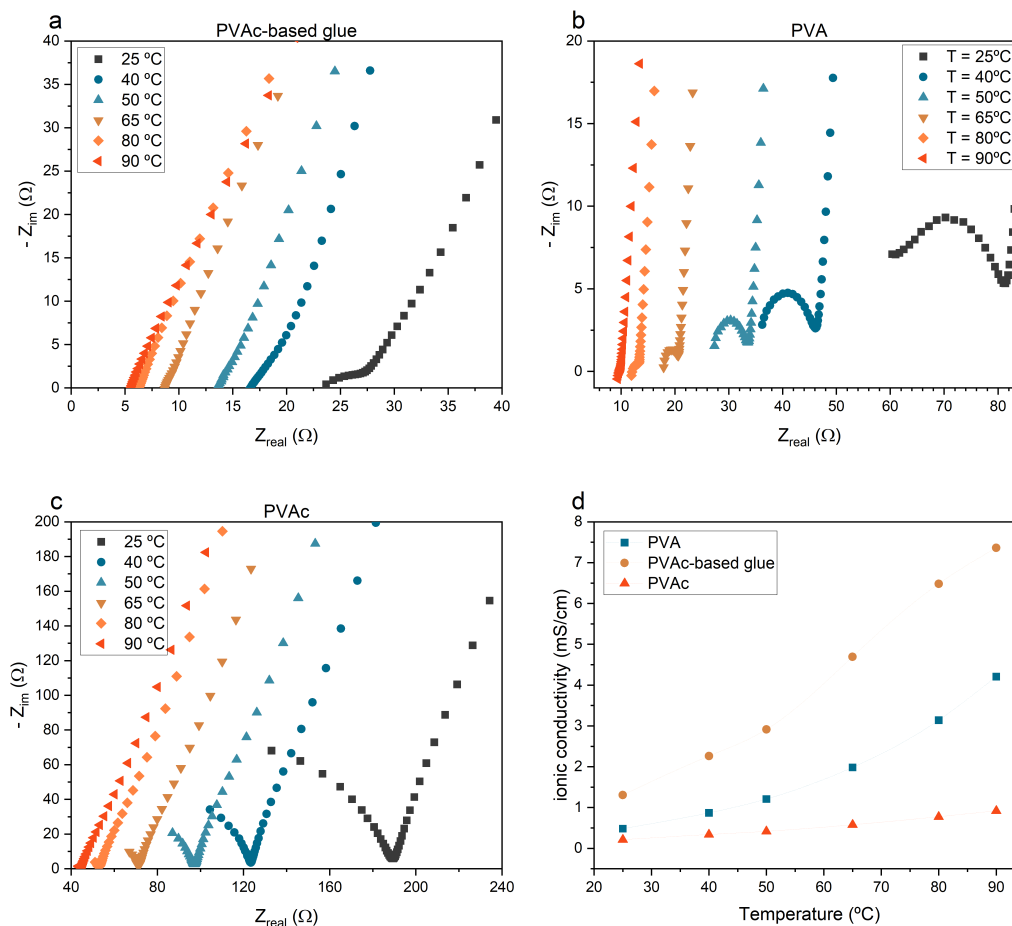


Figure 4. Nyquist diagrams for the Au/NZSP+polymer/Au cells employing (a) PVAc-based glue, (b) PVA, (c) PVAc in the 25 to 90 °C temperature range. (d) Ionic conductivity for each wetting agent as a function of temperature

In addition to testing at high temperatures, low temperature performance is also of interest for applications in near and below-freezing environments, where batteries typically tend to struggle [41]. The same battery test chamber was used as before, this time in the -10 °C to $+20$ °C temperature range. The results, displayed in Figure 5, show a gradual increase in interfacial resistance, accompanied by a reduction in ionic conductivity, as the temperature decreases, for the PVAc-based glue. The lowest value reached at -10 °C of 0.205 mS cm^{-1} represents a 78.5% decrease compared to the conductivity at 20 °C. Noteworthy, this value is still 522 times larger than that of pristine NZSP at room temperature, and of the order of magnitude of PVAc and PVA at room temperature, meaning the PVAc-based glue still performs exceedingly well as a wetting agent, even at below-freezing temperatures. Furthermore, when returning to ambient temperature after the test had concluded, the cell employing PVAc-based glue was able to maintain a performance close to the baseline measured before testing (Figure A1), meaning that the decrease in performance due to exposure to extreme temperatures is a reversible process.

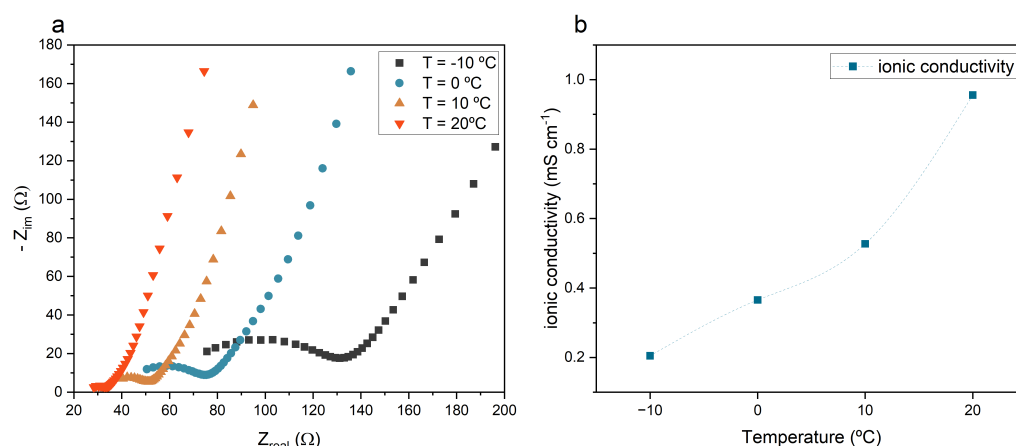


Figure 5. Low temperature testing performance for Au/NZSP+polymer/Au cell using PVAc-based glue displayed in the form of (a) Nyquist diagrams as a function of temperature and (b) ionic conductivity as a function of temperature.

3.4. Na-Ion Full Cell Internal Resistance

Building on the findings from the previous sections, EIS tests were performed on a Na-ion solid-state full cell employing a hard carbon (HC) anode, a carbon coated sodium vanadium phosphate ($\text{Na}_3\text{V}_2(\text{PO}_4)_3$) cathode, and the developed composite NZSP + PVAc-based glue electrolyte.

NVP is an orthophosphate polyanionic compound with NASICON structure that has been identified as one of the most promising cathode materials for sodium-ion batteries. NVP has a high theoretical capacity of 117.6 mAh/g, rich Na^+ transport channels, and high structural stability and rate capability [42,43]. NVP typically lacks electronic conductivity, but this drawback can be effectively mitigated by mixing or applying a coating of a conductive carbon layer, forming a new composite material: NVP/C [44]. A sodiated version of NVP/C has been demonstrated by Ruan et al. to work well with the NZSP solid electrolyte, against Na metal, achieving a discharge capacity of 81.6 mA h/g at a current density of 20 mA/g, dropping to 62.23 mAh/g after 50 cycles [9]. Hard carbon, an insertion-type carbon-based material, was chosen as the anode due to the ease of manufacture and procurement of precursor materials, low working potential, and a high sodium storage capacity of approximately 300 mAh/g [45].

NVP/C powder was prepared using a carbothermal reduction method, followed by calcination [44,46]. NH_4VO_3 , $\text{C}_2\text{H}_2\text{O}_4$, and NaH_2PO_4 were dissolved in deionized water and stirred at 80 °C for 5 h. The obtained gel was dried in an oven under vacuum at 120 °C for 12 h, after which the resulting powder was calcined at 800 °C for 6 h under Ar atmosphere. Both the cathode and the anode were prepared by mixing the active material (NVP/c for the cathode and HC for the anode) with polyvinylidene fluoride (PVDF) and carbon black in a 8:1:1 mass ratio and using NMP as a solvent to produce a slurry that was then coated onto stainless steel current collectors using the doctor blade technique.

The Na-ion full cell Nyquist plot obtained at room temperature, displayed in Figure 6, shows one high frequency z' axis intercept, followed by two semicircles and a linear tail at low frequency. This second semicircle is reflected in the new equivalent circuit that now encompasses a second resistor/CPE parallel element that accounts for the fact that the electrodes are no longer ion-blocking, so a resistance is attributed to the EDLC arising from the intercalation/deintercalation of charges into the porous electrodes [37].

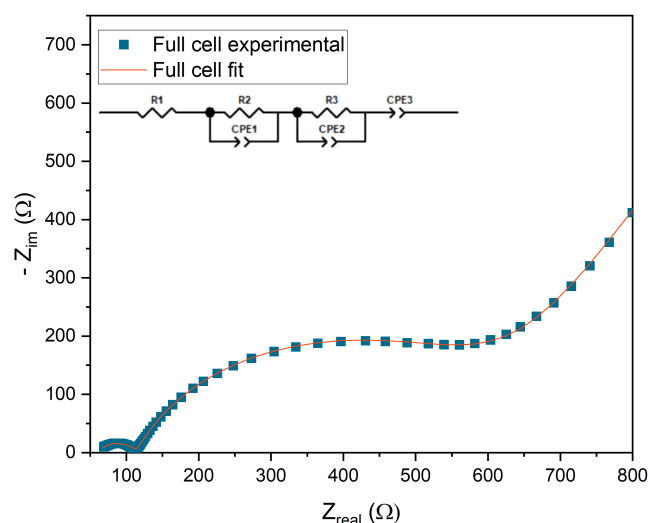


Figure 6. NVP /C//NZSP + PVAc-based glue//HC Na-ion solid-state full cell Nyquist plot, with equivalent circuit model inset

As before, by adding the values of all the resistance contributions (R_1 , R_2 , R_3), the total resistance of $R_t = 653.14 \Omega$ was calculated. Given the dimensions of the solid electrolyte pellet (3.14 cm^{-2}), this value corresponds to an area-specific resistance (ASR) of $2052 \Omega \text{ cm}^2$, substantially lower than that obtained by Jin Oh et al. of $5242 \Omega \text{ cm}^2$ with a similar full cell configuration of NVP/NZSP+PEO/Na [37]. This result offers further validation of the remarkable role of PVAc-based glue as a simple, cost-effective, high-performing wetting agent for Na-ion solid-state batteries with an NZSP solid electrolyte.

4. Conclusions

Solid-state electrolytes play a critical role in advancing battery technology, where solid-state sodium-ion batteries are appealing due to the abundance, affordability, and environmental friendliness of sodium. However, they encounter hurdles such as limited ionic conductivity and high interfacial resistance at the electrode/electrolyte interface, which limits their performance. This study investigates the use of polyvinyl-based polymers as wetting agents to enhance the functionality of the sodium super ionic conductor (NASICON-type) NZSP ($\text{Na}_3\text{Zr}_2\text{Si}_2\text{PO}_{12}$) solid electrolyte, forming a new composite electrolyte with reduced interfacial resistance and improved ionic conductivity. Through EIS testing of several Au/NZSP+wetting agent/Au symmetric cells, PVAc-based commercial glue emerged as the most effective wetting agent, with the composite exhibiting a remarkable ionic conductivity of 1.31 mS cm^{-1} at ambient temperature, 63.8% higher than the pristine NZSP. Moreover, the PVAc-based glue was able to maintain a high ionic conductivity and stability over a large temperature range, from $-10 \text{ }^\circ\text{C}$ to $90 \text{ }^\circ\text{C}$, where an exceptional value of 7.36 mS cm^{-1} was obtained. Finally, a solid-state sodium-ion full cell with NVP/C cathode and HC anode, using the NZSP+PVAc-based glue composite electrolyte showed a low total resistance (ASR) of $2052 \Omega \text{ cm}^2$. The results presented underscore the potential of polyvinyl-based polymers, particularly PVAc-based glue, as a cost-effective, adaptable, stable, and high-performing wetting agent for NZSP, with significant implications for the advancement of solid-state sodium-ion batteries, offering a pathway towards improved performance and viability of these sustainable energy storage solutions.

Author Contributions: Conceptualization, T.A.S., J.V. and J.O.; methodology, T.A.S., J.V., R.C.V. and J.O.; validation, J.V. and J.O.; formal analysis, T.A.S., R.C.V. and J.O.; investigation, T.A.S., J.V., R.C.V. and J.O.; resources, J.V., F.D. and J.O.; data curation, T.A.S., J.V., R.C.V. and J.O.; writing—original draft prepa-

ration, T.A.S., J.V., R.C.V. and J.O.; writing—review and editing, T.A.S., R.C.V., J.V., F.D. and J.O.; supervision, J.V. and J.O. All authors have read and agreed to the published version of the manuscript.

Funding: The authors T.A.S. and J.O. would like to acknowledge the Portuguese Foundation for Science and Technology (FCT) for its financial support via the UIDP/50022/2020 project (LAETA Programmatic Funding); R.C.V. would like to acknowledge the support of FCT—Fundação para a Ciência e a Tecnologia for the funding of the Doctoral Grant SFRH/BD/148785/2019; J.V. would like to acknowledge the funding from FCT through the projects 2022.05030.PTDC and UIDB/04968/2020

Data Availability Statement: The raw data supporting the conclusions of this article will be made available by the authors on request.

Conflicts of Interest: The authors declare no conflicts of interest.

Abbreviations

The following abbreviations are used in this manuscript:

SSIB	Solid-state sodium-ion battery
NASICON	Sodium super ionic conductor
NZSP	$\text{Na}_3\text{Zr}_2\text{Si}_2\text{PO}_{12}$
FTIR-ATR	Fourier transform infrared—attenuated total reflection
PVA	Poly(vinyl alcohol)
PVAc	Poly(vinyl acetate)
CPE	Constant phase element
EIS	Electrochemical impedance spectroscopy
EDS	Energy-dispersive X-ray spectroscopy
SEM	Scanning electron microscopy
NVP	Sodium vanadium phosphate ($\text{Na}_3\text{V}_2(\text{PO}_4)_3$)
HC	Hard carbon
ASR	Area-specific resistance

Appendix A

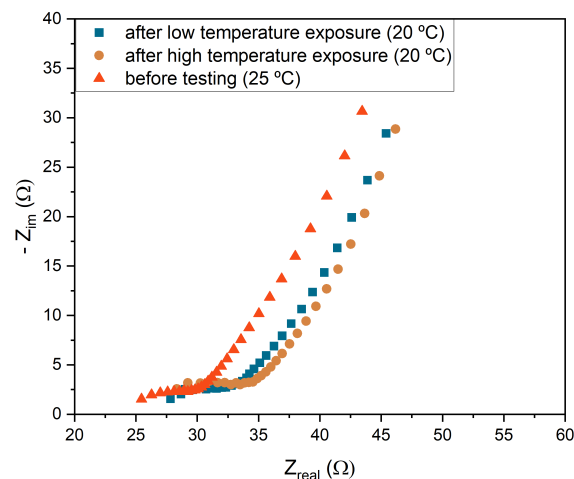


Figure A1. EIS spectra of the same symmetric cell employing PVAc-based glue as a wetting agent before any testing (measured at 25 °C), after testing with high temperatures (measured at 20 °C), and after testing with low temperatures (measured at 20 °C).

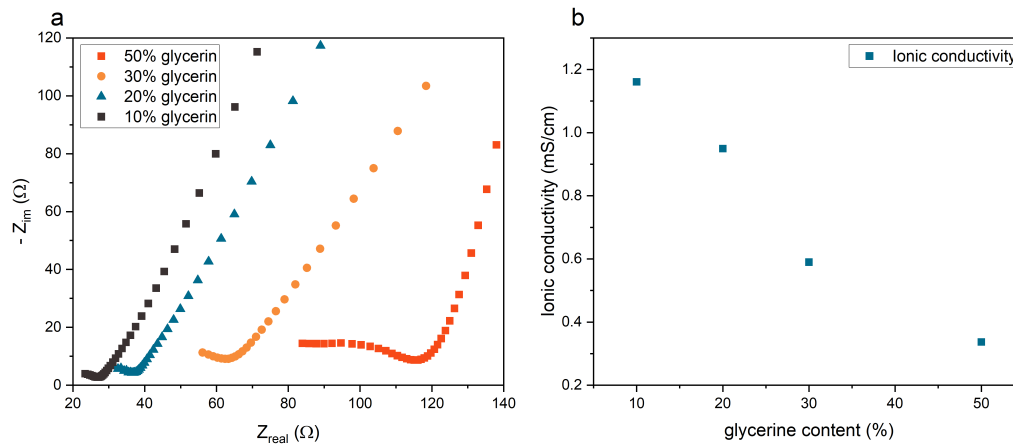


Figure A2. (a) Nyquist diagrams for PVAc-based glue/glycerin mixture, with 10%, 20%, 30%, and 50% glycerin content. (b) Ionic conductivity for each glycerin percentage

Table A1. Fitting parameters for the Nyquist plots presented in Figures 2, 4, and 5. R1 and R2 represent the impedance, in Ω , of the resistive elements of the equivalent circuit. The impedance of a constant phase element is given by the expression $Z = (1/Y_0)(j\omega)^a$. Yo1 and Yo2 represent the capacitance of the constant phase element components, and a1 and a2 represent the exponent, which is =1 for a perfect capacitor and <1 for a CPE [47].

Material	Temp. (°C)	R1 (Ω)	R2 (Ω)	CPE1		CPE2		
				Yo1 ($S \cdot s^a$)	a1	Yo2 ($S \cdot s^a$)	a2	
Pristine NZSP	25	4.05×10^{-3}	6.77×10^4	2.93×10^{-10}	0.85	1.27×10^{-7}	0.68	
	-10	1.43×10^{-4}	199.00	8.12×10^{-5}	0.29	6.74×10^{-6}	0.88	
	0	6.04×10^{-5}	111.60	1.76×10^{-4}	0.26	7.63×10^{-6}	0.88	
	10	1.79×10^{-4}	77.40	5.12×10^{-4}	0.20	8.72×10^{-6}	0.87	
	20	18.77	23.92	4.73×10^{-4}	0.30	1.06×10^{-5}	0.86	
	25	23.66	7.57	2.63×10^{-4}	0.49	1.71×10^{-5}	0.84	
	40	16.41	1.65	1.86×10^{-6}	1.00	1.89×10^{-5}	0.82	
	50	13.51	0.50	1.09×10^{-5}	1.00	2.66×10^{-5}	0.81	
	65	8.639	0.05	1.21×10^{-3}	0.09	2.86×10^{-5}	0.81	
	80	6.295	4.51×10^{-5}	8.98×10^{-5}	0.84	2.98×10^{-5}	0.82	
PVAc-based glue coating	25	52.48	32.02	3.74×10^{-6}	0.62	8.21×10^{-6}	0.93	
	40	34.14	12.84	6.75×10^{-7}	0.79	9.46×10^{-6}	0.92	
	50	26.68	7.09	1.90×10^{-7}	0.90	1.04×10^{-5}	0.91	
	65	20.57	0.04	2.93×10^{-5}	0.89	1.95×10^{-5}	0.91	
	80	13.00	0.03	3.42×10^{-5}	0.87	2.15×10^{-5}	0.90	
	90	9.70	0.01	5.85×10^{-5}	0.85	1.78×10^{-5}	0.88	
	Pure PVA coating	25	52.48	32.02	3.74×10^{-6}	0.62	8.21×10^{-6}	0.93
		40	34.14	12.84	6.75×10^{-7}	0.79	9.46×10^{-6}	0.92
		50	26.68	7.09	1.90×10^{-7}	0.90	1.04×10^{-5}	0.91
		65	20.57	0.04	2.93×10^{-5}	0.89	1.95×10^{-5}	0.91
80		13.00	0.03	3.42×10^{-5}	0.87	2.15×10^{-5}	0.90	

Table A1. Cont.

Material	Temp. (°C)	R1 (Ω)	R2 (Ω)	CPE1		CPE2	
				Yo1 (S·s ^a)	a1	Yo2 (S·s ^a)	a2
Pure PVAc coating	25	29.35	163.30	5.47×10^{-9}	0.87	1.83×10^{-5}	0.89
	40	120.8	0.08	4.40×10^{-5}	0.97	3.98×10^{-5}	0.82
	50	3.966	94.16	7.22×10^{-9}	0.82	2.55×10^{-5}	0.85
	65	70.86	0.02	5.77×10^{-5}	1.00	4.80×10^{-5}	0.79
	80	52.69	0.01	6.51×10^{-5}	0.94	6.37×10^{-5}	0.77
	90	44.29	0.01	7.60×10^{-5}	0.89	8.11×10^{-5}	0.76

References

- Chaves, C.; Pereira, E.; Ferreira, P.; Dias, A.G. Concerns about lithium extraction: A review and application for Portugal. *Extr. Ind. Soc.* **2021**, *8*, 100928. [\[CrossRef\]](#)
- Peters, J.F.; Cruz, A.P.; Weil, M. Exploring the Economic Potential of Sodium-Ion Batteries. *Batteries* **2019**, *5*, 10. [\[CrossRef\]](#)
- Tian, Y.; Zeng, G.; Rutt, A.; Shi, T.; Kim, H.; Wang, J.; Koettgen, J.; Sun, Y.; Ouyang, B.; Chen, T.; et al. Promises and Challenges of Next-Generation “beyond Li-ion” Batteries for Electric Vehicles and Grid Decarbonization. *Chem. Rev.* **2021**, *121*, 1623–1669. [\[CrossRef\]](#) [\[PubMed\]](#)
- Hwang, J.Y.; Myung, S.T.; Sun, Y.K. Sodium-ion batteries: Present and future. *Chem. Soc. Rev.* **2017**, *46*, 3529–3614. [\[CrossRef\]](#) [\[PubMed\]](#)
- Li, Z.; Liu, P.; Zhu, K.; Zhang, Z.; Si, Y.; Wang, Y.; Jiao, L. Solid-State Electrolytes for Sodium Metal Batteries. *Energy Fuels* **2021**, *35*, 9063–9079. [\[CrossRef\]](#)
- Tarascon, J.M. Na-ion versus Li-ion Batteries: Complementarity Rather than Competitiveness. *Joule* **2020**, *4*, 1616–1620. [\[CrossRef\]](#)
- Ahmad, H.; Kubra, K.T.; Butt, A.; Nisar, U.; Iftikhar, F.J.; Ali, G. Recent progress, challenges, and perspectives in the development of solid-state electrolytes for sodium batteries. *J. Power Sources* **2023**, *581*, 233518. [\[CrossRef\]](#)
- Goodenough, J.B.; Hong, H.Y.; Kafalas, J.A. Fast Na⁺-ion transport in skeleton structures. *Mater. Res. Bull.* **1976**, *11*, 203–220. [\[CrossRef\]](#)
- Ruan, Y.; Guo, F.; Liu, J.; Song, S.; Jiang, N.; Cheng, B. Optimization of Na₃Zr₂Si₂PO₁₂ ceramic electrolyte and interface for high performance solid-state sodium battery. *Ceram. Int.* **2019**, *45*, 1770–1776. [\[CrossRef\]](#)
- Hwang, S.M.; Park, J.S.; Kim, Y.; Go, W.; Han, J.; Kim, Y.; Kim, Y. Rechargeable Seawater Batteries—From Concept to Applications. *Adv. Mater.* **2019**, *31*, 1804936. [\[CrossRef\]](#)
- Zhang, Q.; Zhou, Q.; Lu, Y.; Shao, Y.; Qi, Y.; Qi, X.; Zhong, G.; Yang, Y.; Chen, L.; Hu, Y.S. Modification of NASICON Electrolyte and Its Application in Real Na-Ion Cells. *Engineering* **2022**, *8*, 170–180. [\[CrossRef\]](#)
- Lee, J.S.; Chang, C.M.; Lee, Y.I.; Lee, J.H.; Hong, S.H. Spark Plasma Sintering (SPS) of NASICON Ceramics. *J. Am. Ceram. Soc.* **2004**, *87*, 305–307. [\[CrossRef\]](#)
- Zhang, Q.; Lu, Y.; Guo, W.; Shao, Y.; Liu, L.; Lu, J.; Rong, X.; Han, X.; Li, H.; Chen, L.; et al. Hunting Sodium Dendrites in NASICON-Based Solid-State Electrolytes. *Energy Mater. Adv.* **2021**, *2021*, 9870879. [\[CrossRef\]](#)
- Li, C.; Li, R.; Liu, K.; Si, R.; Zhang, Z.; Hu, Y. NaSICON: A promising solid electrolyte for solid-state sodium batteries. *Interdiscip. Mater.* **2022**, *1*, 396–416. [\[CrossRef\]](#)
- Ferreira, J.; Salgueiro, T.; Marcuzzo, J.; Arruda, E.; Ventura, J.; Oliveira, J. Textile PAN Carbon Fibers Cathode for High-Voltage Seawater Batteries. *Batteries* **2023**, *9*, 178. [\[CrossRef\]](#)
- Leng, H.; Huang, J.; Nie, J.; Luo, J. Cold sintering and ionic conductivities of Na_{3.256}Mg_{0.128}Zr_{1.872}Si₂PO₁₂ solid electrolytes. *J. Power Sources* **2018**, *391*, 170–179. [\[CrossRef\]](#)
- Zhang, L.; Liu, Y.; You, Y.; Vinu, A.; Mai, L.; You, C.Y. NASICONs-type solid-state electrolytes: The history, physicochemical properties, and challenges. *Interdiscip. Mater.* **2023**, *2*, 91–110. [\[CrossRef\]](#)
- Fu, Y.; Liu, D.; Sun, Y.; Zhao, G.; Guo, H. Epoxy Resin-Reinforced F-Assisted Na₃Zr₂Si₂PO₁₂ Solid Electrolyte for Solid-State Sodium Metal Batteries. *Batteries* **2023**, *9*, 331. [\[CrossRef\]](#)
- Zhao, C.; Liu, L.; Qi, X.; Lu, Y.; Wu, F.; Zhao, J.; Yu, Y.; Hu, Y.S.; Chen, L. Solid-State Sodium Batteries. *Adv. Energy Mater.* **2018**, *8*, 1703012. [\[CrossRef\]](#)
- Aziz, S.B.; Nofal, M.M.; Abdulwahid, R.T.; Ghareeb, H.O.; Dannoun, E.M.; Abdullah, R.M.; Hamsan, M.H.; Kadir, M.F. Plasticized Sodium-Ion Conducting PVA Based Polymer Electrolyte for Electrochemical Energy Storage—EEC Modeling, Transport Properties, and Charge-Discharge Characteristics. *Polymers* **2021**, *13*, 803. [\[CrossRef\]](#)
- Gebert, F.; Knott, J.; Gorkin, R.; Chou, S.L.; Dou, S.X. Polymer electrolytes for sodium-ion batteries. *Energy Storage Mater.* **2021**, *36*, 10–30. [\[CrossRef\]](#)

22. Bhargav, P.B.; Mohan, V.M.; Sharma, A.K.; Rao, V.V. Characterization of poly(vinyl alcohol)/sodium bromide polymer electrolytes for electrochemical cell applications. *J. Appl. Polym. Sci.* **2008**, *108*, 510–517. [CrossRef]
23. Sasikumar, M.; Jagadeesan, A.; Raja, M.; Krishna, R.H.; Sivakumar, P. The effects of PVAc on surface morphological and electrochemical performance of P(VdF-HFP)-based blend solid polymer electrolytes for lithium ion-battery applications. *Ionics* **2019**, *25*, 2171–2181. [CrossRef]
24. Navaratnam, S.; Rahman, N.A.A.; Idris, N.A.; Abidin, S.Z.Z. The Effect of Glycerol on Na + Ion Conductivity and Dielectric Properties of Potato Starch-Chitosan Blend Biopolymer Electrolyte. *Int. J. Electroact. Mater* **2020**, *8*, 10–18.
25. 4 to One Co., L. Seawater Battery Materials. Available online: https://www.4toone.com/modules/catalogue2_product/cg_view.html?cc=1010&p=1&no=5 (accessed on 10 February 2024).
26. Kim, J.K.; Mueller, F.; Kim, H.; Bresser, D.; Park, J.S.; Lim, D.H.; Kim, G.T.; Passerini, S.; Kim, Y. Rechargeable-hybrid-seawater fuel cell. *NPG Asia Mater.* **2014**, *6*, e144. [CrossRef]
27. Vadhva, P.; Hu, J.; Johnson, M.J.; Stocker, R.; Braglia, M.; Brett, D.J.; Rettie, A.J. Electrochemical Impedance Spectroscopy for All-Solid-State Batteries: Theory, Methods and Future Outlook. *ChemElectroChem* **2021**, *8*, 1930–1947. [CrossRef]
28. Abdelghany, A.M.; Meikhal, M.S.; Asker, N. Synthesis and structural-biological correlation of PVC/PVAc polymer blends. *J. Mater. Res. Technol.* **2019**, *8*, 3908–3916. [CrossRef]
29. Debuigne, A.; Caille, J.R.; Willet, N.; Jérôme, R. Synthesis of Poly(vinyl acetate) and Poly(vinyl alcohol) Containing Block Copolymers by Combination of Cobalt-Mediated Radical Polymerization and ATRP. *Macromolecules* **2005**, *38*, 9488–9496. [CrossRef]
30. Acik, G.; Cansoy, C.E.; Kamaci, M. Effect of flow rate on wetting and optical properties of electrospun poly(vinyl acetate) micro-fibers. *Colloid Polym. Sci.* **2019**, *297*, 77–83. [CrossRef]
31. Căprărescu, S.; Modrogan, C.; Purcar, V.; Dăncilă, A.M.; Orbuleț, O.D. Study of Polyvinyl Alcohol-SiO₂ Nanoparticles Polymeric Membrane in Wastewater Treatment Containing Zinc Ions. *Polymers* **2021**, *13*, 1875. [CrossRef]
32. Teixeira, J.S.; Pereira, A.M.; Pereira, C. Smart dual-functional energy storage/fluorescent textile device based on a new redox-active Mn-doped ZnS solid-gel electrolyte. *Chem. Eng. J.* **2021**, *426*, 131274. [CrossRef]
33. Mansur, H.S.; Sadahira, C.M.; Souza, A.N.; Mansur, A.A. FTIR spectroscopy characterization of poly (vinyl alcohol) hydrogel with different hydrolysis degree and chemically crosslinked with glutaraldehyde. *Mater. Sci. Eng. C* **2008**, *28*, 539–548. [CrossRef]
34. Rajendran, S.; Sivakumar, M.; Subadevi, R. Investigations on the effect of various plasticizers in PVA–PMMA solid polymer blend electrolytes. *Mater. Lett.* **2004**, *58*, 641–649. [CrossRef]
35. Saffirio, S.; Falco, M.; Appetecchi, G.B.; Smeacetto, F.; Gerbaldi, C. Li_{1.4}Al_{0.4}Ge_{0.4}Ti_{1.4}(PO₄)₃ promising NASICON-structured glass-ceramic electrolyte for all-solid-state Li-based batteries: Unravelling the effect of diboron trioxide. *J. Eur. Ceram. Soc.* **2022**, *42*, 1023–1032. [CrossRef]
36. Wen, C.; Luo, Z.; Liu, X.; Wu, Y.; Tong, J.; Liang, H.; Zhang, Q.; Ning, T.; Lu, A. Enhanced electrochemical properties of NASICON-type Na₃Zr₂Si₂PO₁₂ solid electrolytes with Tb³⁺-ions-assisted sintering. *Solid State Ionics* **2023**, *393*, 116185. [CrossRef]
37. Oh, J.A.S.; Xu, X.; Zeng, Z.; Wang, K.; Tan, N.Y.J.; Kok, E.; Huang, J.; Lu, L. Thin NASICON Electrolyte to Realize High Energy Density Solid-State Sodium Metal Battery. *Energy Environ. Mater.* **2023**, *6*, e12472. [CrossRef]
38. Zhou, W.; Wang, S.; Li, Y.; Xin, S.; Manthiram, A.; Goodenough, J.B. Plating a Dendrite-Free Lithium Anode with a Polymer/Ceramic/Polymer Sandwich Electrolyte. *J. Am. Chem. Soc.* **2016**, *138*, 9385–9388. [CrossRef] [PubMed]
39. Tsiptsias, C.; Fardis, D.; Ntampou, X.; Tsvintzelis, I.; Panayiotou, C. Thermal Behavior of Poly(vinyl alcohol) in the Form of Physically Crosslinked Film. *Polymers* **2023**, *15*, 1843. [CrossRef]
40. Liu, P.; Chen, W.; Liu, C.; Tian, M.; Liu, P. A novel poly (vinyl alcohol)/poly (ethylene glycol) scaffold for tissue engineering with a unique bimodal open-celled structure fabricated using supercritical fluid foaming. *Sci. Rep.* **2019**, *9*, 9534. [CrossRef]
41. Wang, M.; Wang, Q.; Ding, X.; Wang, Y.; Xin, Y.; Singh, .P.; Wu, .F.; Gao, H. The prospect and challenges of sodium-ion batteries for low-temperature conditions. *Interdiscip. Mater.* **2022**, *1*, 373–395. [CrossRef]
42. Zeng, X.; Peng, J.; Guo, Y.; Zhu, H.; Huang, X. Research Progress on Na₃V₂(PO₄)₃ Cathode Material of Sodium Ion Battery. *Front. Chem.* **2020**, *8*, 561787. [CrossRef]
43. Akçay, T.; Häringer, M.; Pfeifer, K.; Anhalt, J.; Binder, J.R.; Dsoke, S.; Kramer, D.; Mönig, R. Na₃V₂(PO₄)₃-A Highly Promising Anode and Cathode Material for Sodium-Ion Batteries. *ACS Appl. Energy Mater.* **2021**, *4*, 12688–12695. [CrossRef]
44. Luo, S.H.; Li, J.Y.; Bao, S.; Liu, Y.Y.; Wang, Z. Na₃V₂(PO₄)₃/C Composite Prepared by Sol-Gel Method as Cathode for Sodium Ion Batteries. *J. Electrochem. Soc.* **2018**, *165*, A1460–A1465. [CrossRef]
45. Zhang, T.; Li, C.; Wang, F.; Noori, A.; Mousavi, M.F.; Xia, X.; Zhang, Y. Recent Advances in Carbon Anodes for Sodium-Ion Batteries. *Chem. Rec.* **2022**, *22*, e202200083. [CrossRef]
46. Zhao, Q.; Yang, W.; Zhang, Q.; Qiu, L.; Zhou, M.; Lu, S.; Tao, B.; Wang, X.; Xie, Q.; Ruan, Y. Facile synthesis of pure Na₃V₂(PO₄)₃ powder via a two-stage carbothermal reduction strategy. *J. Sol-Gel Sci. Technol.* **2022**, *103*, 205–213. [CrossRef]
47. Gamry Instruments, Warminster, USA Physical Electrochemistry & Equivalent Circuit Elements, Part 2. Available online: <https://www.gamry.com/assets/White-Papers/The-Basics-of-EIS-Part-2-2.pdf> (accessed on 4 April 2024).

Disclaimer/Publisher’s Note: The statements, opinions and data contained in all publications are solely those of the individual author(s) and contributor(s) and not of MDPI and/or the editor(s). MDPI and/or the editor(s) disclaim responsibility for any injury to people or property resulting from any ideas, methods, instructions or products referred to in the content.